Lithium hydroxide, LiOH, at elevated densities

Andreas Hermann, N. W. Ashcroft, and Roald Hoffmann

Citation: The Journal of Chemical Physics **141**, 024505 (2014); doi: 10.1063/1.4886335
View online: http://dx.doi.org/10.1063/1.4886335
View Table of Contents: http://scitation.aip.org/content/aip/journal/jcp/141/2?ver=pdfcov
Published by the AIP Publishing

Lithium hydroxide, LiOH, at elevated densities

Andreas Hermann,[1] N. W. Ashcroft,[2] and Roald Hoffmann[3]
[1]*School of Physics and Astronomy and Centre for Science at Extreme Conditions, The University of Edinburgh, Edinburgh EH9 3JZ, United Kingdom*
[2]*Laboratory of Atomic and Solid State Physics, Cornell University, Ithaca, New York 14853, USA*
[3]*Department of Chemistry and Chemical Biology, Cornell University, Ithaca, New York 14853, USA*

(Received 30 April 2014; accepted 12 June 2014; published online 9 July 2014)

We discuss the high-pressure phases of crystalline lithium hydroxide, LiOH. Using first-principles calculations, and assisted by evolutionary structure searches, we reproduce the experimentally known phase transition under pressure, but we suggest that the high-pressure phase LiOH-III be assigned to a new hydrogen-bonded tetragonal structure type that is unique amongst alkali hydroxides. LiOH is at the intersection of both ionic and hydrogen bonding, and we examine the various ensuing structural features and their energetic driving mechanisms. At P = 17 GPa, we predict another phase transition to a new phase, *Pbcm*-LiOH-IV, which we find to be stable over a wide pressure range. Eventually, at extremely high pressures of 1100 GPa, the ground state of LiOH is predicted to become a polymeric structure with an unusual graphitic oxygen-hydrogen net. However, because of its ionic character, the anticipated metallization of LiOH is much delayed; in fact, its electronic band gap increases monotonically into the TPa pressure range. © *2014 AIP Publishing LLC*. [http://dx.doi.org/10.1063/1.4886335]

I. INTRODUCTION

Lithium hydroxide, LiOH, is a light element compound at the crossroads of molecular and ionic bonding. The metastable monomeric molecule is linear (as is LiOLi, but not HOH), yet quite non-rigid. At 298 K (and below) and P = 1 atm, LiOH is a hygroscopic ionic solid. Anhydrous LiOH at P = 1 atm is relatively stable, melting at 462 °C, attesting to its ionic character. It finds use in tight spaces: as precursor of lithium greases such as lithium stearate,[1] and as a carbon dioxide absorbant in spacecrafts or submarines (converting CO_2 to lithium carbonate).[2,3] Hydrated LiOH exists, as the monohydrate $LiOH \cdot H_2O$, the X-ray and neutron crystal structures of which are available.[4,5]

In the solid state anhydrous LiOH, unlike water ice, for instance, does not feature a hydrogen bonding network; the absence of such bonding in the solid at room temperature is in line with other alkali metal hydroxides (and also amides).[6–12]

Yet hydrogen bonding is lurking as the fate of these materials as one moves to lower temperature or higher pressure. Phase transitions in many of the associated compounds to hydrogen-bonded or even polymeric anionic structures are observed or predicted.[7–10,13–23] In the present study, we investigate the influence of compression on the structural and electronic properties of LiOH. We find that LiOH takes a unique pathway amongst its isoelectronic or isolobal analogues, by forming a network structure of linear hydrogen bonds at moderate pressures, before more compact structures of hydrogen-bonded zig-zag chains and eventual polymeric structures are stabilized at very high pressures. We will make a case below for reconsideration of previous experimental and computational assignment of the intermediate-pressure phase of LiOH.

Another motivation of this work comes from our recent studies of the high-pressure phases of water ice, where we asked what pressure would be needed to metallize H_2O.[24–26] As it turned out, the metallization pressure of ice is very likely to be high, around 5TPa, and thus larger than the pressures found even in the core of Jupiter. One might ask, however, if metallization of ice could be induced at lower pressure by addition or substitution of an electropositive element, such as an alkali or alkaline earth metal—as is predicted, for example, for hydrogen, where metallic polyhydride phases are proposed to be stabilized under pressure.[27–31] Here we study partial substitution of lithium in H_2O, which naturally leads one to both anhydrous LiOH (replacing every second H by Li), and the monohydrate $LiOH{+}H_2O$ (replacing every fourth H by Li).

II. SOLID LIOH AT ATMOSPHERIC PRESSURE

At atmospheric pressure and room temperature, LiOH crystallizes in a tetragonal structure of *P4/nmm* symmetry with two formula units per unit cell.[6,32,33] The structure comprises layers of square lattices of lithium atoms, with each square capped by a hydroxide ion, alternating above and below the lithium layer (see Figure 1). Thus, each oxygen ion is fourfold coordinated with lithium atoms, and each lithium atom is in a distorted tetrahedral environment of oxygen atoms.

The hydroxyl groups in LiOH do not form hydrogen bonds, which is also the case for the solids of the heavier alkali hydroxides (i.e., MOH with M = Na, K, Rb, or Cs) at room temperature. However, almost all of those exhibit a low temperature phase, where the OH groups arrange themselves to form hydrogen-bonded zig-zag chains

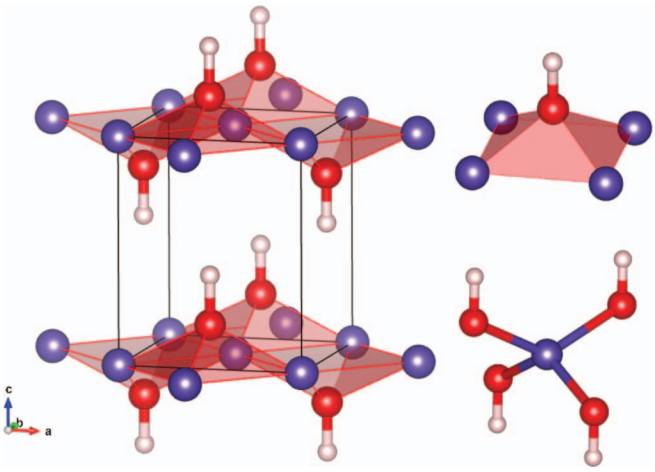

FIG. 1. Left: the *P4/nmm* ground-state static structure of LiOH-II at P = 1 atm. Red (white, purple) spheres denote O (H, Li) atoms. OH groups and O-Li coordination polyhedra are indicated. Right: coordination polyhedra of OH and Li, respectively.

O–H · · · O-H · · · O–H, in macroscopic antiferroelectric order.[7–10,15–17,34] A peculiar case is NaOH, which does not exhibit such a phase transition, while its deuterated analogue, NaOD, does; it has been argued that tunnelling of the protons in NaOH prevent the phase transition.[7,35] In LiOH the *P4/nmm* phase is stable down to at least 10 K.[36] It is designated as LiOH-II, while a high-temperature phase of unknown structure is designated as LiOH-I.[36,37]

The absence of hydrogen bonds in room temperature alkali hydroxides (and LiOH at all temperatures) is curious. One argument for the structural choices in these compounds is that the protons of the OH groups benefit from maximizing their separation from the positively charged cations, which in turn benefit from close proximity to the negatively charged oxygen atoms. That favors a layered structure with outward-pointing OH groups. These could then only establish hydrogen bonds to adjacent layers, and would require tilting of the OH groups away from the *c* axis; in itself this is not an issue, but it reduces the proton-cation separation. This seems energetically unfavorable for LiOH, but is possible for the heavier alkali hydroxides, where the proton-cation separations are larger. At finite temperature, however, tunnelling and rotational degrees of freedom of the OH groups are unlocked, and the hydrogen bond network is lost (or at least significantly weakened).

Another way of thinking about this starts with the atoms: these compounds are very ionic, and protons are very small. An educated guess for the alkali-oxygen sublattice would be the rocksalt structure, but there are then no obvious sites for the protons that maximize the proton-cation separation. Hence the rocksalt structure is broken up, elongated along the *c* axis, until it reduces to a layered (or bilayered) structure; protons can then be inserted in a very convenient way between the layers, forming hydroxyl groups in the process. Additional degrees of freedom such as shifting of adjacent layers within the *ab* plane lead to the structural variety seen for the different alkali metals.

While there are no hydrogen bonds in LiOH, does not one have "lithium-bonds"? These have been discussed in the literature,[38–40] as there is little question that naked lithium atoms in molecules have a great, great proclivity for electron pairs—if there is a nitrogen or oxygen base with available lone pairs of electrons in the vicinity, lithium atoms bound to other atoms will associate with such Lewis bases. The LiOH solid state structure certainly shows each Li^+ coordinated to four oxygens of OH^- group around it. So perhaps a fair comparison to make with the structure of water ice is that LiOH in the solid forms four Li · · · O "lithium bonds" per lithium, but no H · · · O hydrogen bonds.

III. HIGHER-DENSITY PHASE TRANSITION IN LIOH

Can pressure induce a phase transition in LiOH that leads to the formation of hydrogen bonds? This is certainly true for the heavier alkali hydroxides, all of which exhibit (at room temperature) a transition to their respective low-temperature phases at moderate pressures of 0.7–0.9 GPa.[20,21,41,42] Remarkably, also NaOH (which does not have such a low-temperature phase) forms a hydrogen-bonded structure under pressure, which is a distorted NiAs structure of *Pbcm* symmetry.[20,21] It is thus reasonable to assume a similar progression of phases in LiOH—and indeed, both IR/Raman spectroscopy and powder neutron diffraction experiments indicated a clear phase transition to a new phase, coined LiOH-III, at 0.7 GPa (and 1.7 GPa in LiOD).[18,19] LiOH-III is characterized by a significant reduction (softening) of the symmetric and asymmetric O-H stretching frequencies and a significant volume reduction when compared with LiOH-II.

LiOH-III was initially suggested to possess the *Pbcm* symmetry with a doubled unit cell compared to *P4/nmm*-LiOH-II,[18] but the room-temperature neutron data were eventually fitted to a monoclinic structure of $P2_1/a$ symmetry, inspired by the low-temperature modification of NaOD.[19] A subsequent computational study using the metadynamics approach[43,44] to explore the potential energy surface of LiOH found that a quasi-monoclinic phase, which featured zig-zag hydrogen bonds between the OH groups, was stabilized at elevated pressures.[45] This phase, however, was found at much higher pressures than the experimental phase LiOH-III; its structure factor did not agree very well with the experimental neutron pattern; and the softening of the O-D stretching mode with pressure was an order of magnitude larger than seen in experiment.

IV. STRUCTURE SEARCHES

To find other potential structures of LiOH-III, we performed ground state structure searches using the evolutionary algorithm approach at P = 1 atm, 50 GPa, 100 GPa, and 600 GPa, (corresponding to relative compressions V_0/V of about 2.0, 2.4, and 4.2, respectively) with four formula units per unit cell, respectively, using the XtalOpt methodology interfaced with the VASP density functional package and the projector augmented wave (PAW) approach for the electron-ion interaction[46–49] (see Sec. XI for more details). Candidate structures from each search were optimized across the whole pressure range and to even higher pressures. In Figure 2 we show the relative enthalpy of formation of the ground states

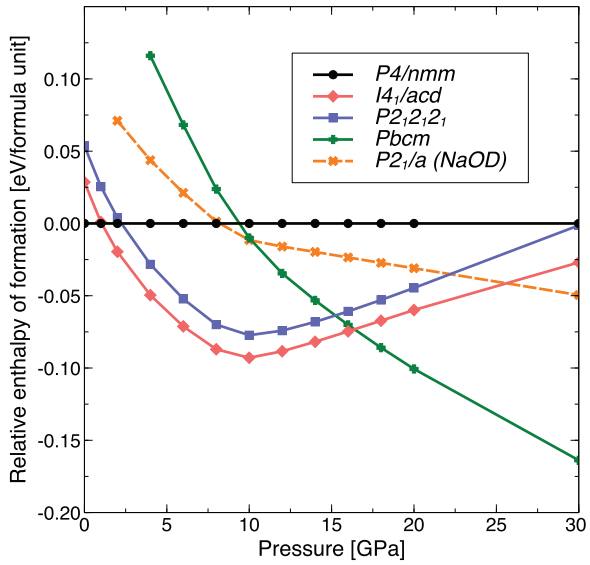

FIG. 2. Relative enthalpy of formation of various static ground state LiOH candidate structures as a function of pressure. The P = 1 atm structure of *P4/nmm* symmetry is the reference.

(not including dynamical effects) of the best structural candidates up to P = 30 GPa, including the structural suggestions for LiOH-III from the aforementioned experimental and computational literature.

Our structure search correctly identifies the experimental *P4/nmm* structure as the global minimum at P = 1 atm, and our optimized ground state structure also agrees well with experimental data, see Table I. At P = 1 GPa, a new phase of $I4_1/acd$ symmetry becomes most stable, and remains the minimum enthalpy structure up to P = 16.5 GPa, where another phase of *Pbcm* symmetry becomes more stable—and remains the most stable phase of LiOH up to about P = 1100 GPa, (relative compression $V_0/V = 5.2$) according to our calculations. The $P2_1/a$ structure suggested by experiment, which is similar to the low-temperature NaOD phase, and was possibly seen in the metadynamics simulations, is not stable at any pressure in our calculations. We therefore argue below that the LiOH-III phase is instead a new structure type amongst the alkali hydroxides, with $I4_1/acd$ symmetry, and yet another phase, LiOH-IV of *Pbcm* symmetry, should be stabilized at pressures higher than 16.5 GPa.

V. REASSIGNMENT OF LIOH-III

We find the $I4_1/acd$ structure to be the most stable ground state structure between P = 1 GPa and P = 16.5 GPa. The *P4/nmm* → $I4_1/acd$ transition pressure agrees well with the experimental transition pressure of 0.7 GPa between LiOH-II and LiOH-III; however, the structure we find is very different from those proposed so far. In Figure 3, we show the $I4_1/acd$ structure; the *local* environment of each atom is in a way very similar to the *P4/nmm* structure: each oxygen atom is the cap of a square pyramid of lithium atoms, and each lithium atom is approximately tetrahedrally coordinated to four oxygen atoms (see Figure 3). In $I4_1/acd$, however, the OH groups form linear O–H · · · O–H · · · O–H · · · chains throughout the lattice: the essential difference between the *P4/nmm* and $I4_1/acd$ structures is the re-orientation of the OH groups, which in *P4/nmm* are all aligned (anti-)parallel, but in $I4_1/acd$ change direction by 90° in successive layers along the *c* axis. This rearrangement of the OH groups allows for a far more compact overall structure: the volume per formula unit in $I4_1/acd$ at P = 2 GPa is 11% smaller than that of *P4/nmm* at the same pressure—and 20% smaller than that of *P4/nmm* at P = 1 atm, in very

TABLE I. Structural properties of relevant low-pressure ground state phases of LiOH, and room temperature neutron diffraction results for LiOH-II at P = 1 atm.

Phase	Pressure	Unit cell [Å]	Atomic positions
P4/nmm	1 atm	a = b = 3.563, c = 4.481	H 2c(1/4,1/4,0.4057) Li 2a(3/4,1/4,0) O 2c(1/4,1/4,0.1892)
	1 atm (Expt.[32])	a = b = 3.557, c = 4.339	H 2c(1/4,1/4,0.407) Li 2a(3/4,1/4,0) O 2c(1/4,1/4,0.194)
$I4_1/acd$	2 GPa	a = b = 5.975, c = 10.228	H 16e(−0.201,0,1/4) Li 8a(0,1/4,3/8) Li 8b(0,1/4,1/8) O 16e(0.463,0,1/4)
$P2_12_12_1$	2 GPa	a = 4.132, b = 3.302, c = 6.634	H 4a(0.4408, −0.1474, −0.2207) Li 4a(−0.4834, 0.0122, 0.1029) O 4a(−0.2335, −0.4936, 0.1474)
$P2_1/a$ (NaOD)	2 GPa	a = 6.014, b = 3.177, c = 5.039, $\beta = 106.02°$	H 4e(0.2747, 0.7766, 0.5927) Li 4e(0.8875, 0.5839, 0.1604) O 4e(0.7826, 0.5522, 0.7569)
Pbcm	20 GPa	a = 2.693, b = 4.838, c = 5.052	H 4d(−0.0693, 0.0410, 1/4) Li 4c(0.3333,1/4,0) O 4d(−0.2255,0.4212,1/4)

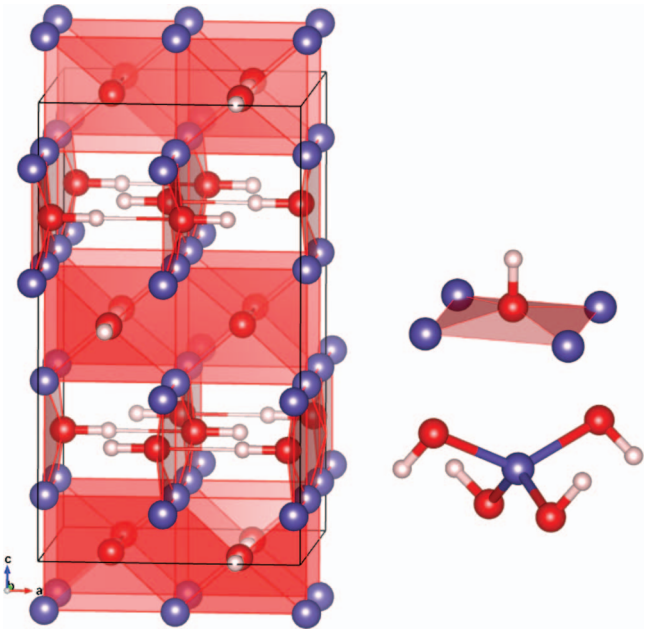

FIG. 3. Left: the $I4_1/acd$ ground state structure of LiOH-III at P = 10 GPa. Thin lines indicate linear OH · · · O hydrogen bonds, atom and polyhedral colors are the same as in Figure 1. Right: coordination polyhedra of OH and Li, respectively.

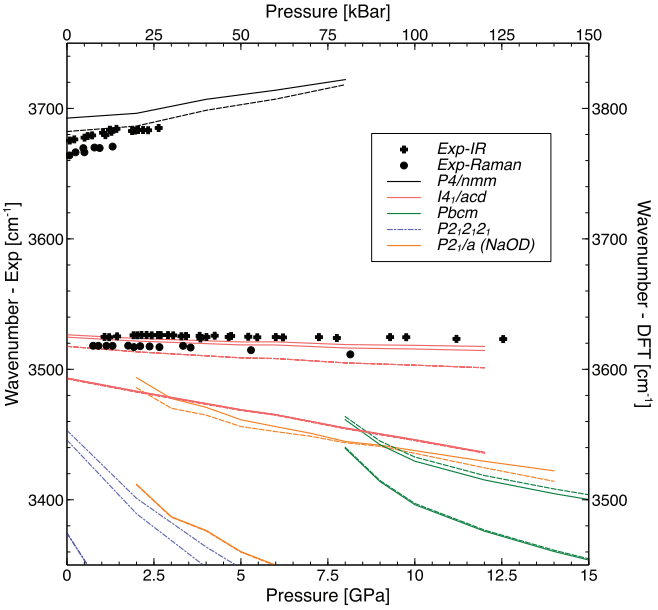

FIG. 4. Calculated IR/Raman spectra for candidate ground state structures of LiOH-III, as compared to room temperature experimental data. Solid (dashed) lines indicate IR (Raman) active modes. All modes in the $P2_12_12_1$ phase are both IR and Raman active. Experimental data from Ref. 18.

good agreement with experiment.[19] In Figure S1 of the supplementary material (SM),[50] we show the volume-pressure relations for the most important of these LiOH structures.

The $I4_1/acd$ structure of LiOH-III has *linear* O–H · · · O–H hydrogen bonds, and these set it apart from all other low-temperature or high-pressure alkali hydroxide structures. The OH · · · O distance varies from 2.00 Å at P = 2 GPa to 1.74 Å at P = 20 GPa. The corresponding hydrogen bond length in ice VIII is a bit shorter in the same pressure range; it varies from 1.88 Å to 1.60 Å. Meanwhile, the covalent O–H bond distance in LiOH remains constant at 0.98 Å (see Figure S2 of the supplementary material[50]).

The hydrogen bonding we observe indeed lowers the O–H stretching frequency, as seen in experiment. We compare the calculated and measured IR/Raman peak positions of LiOH in Figure 4 (note that, because of the anharmonic character of the O–H stretch in LiOH,[51–54] we have shifted the frequency axes of experiment and our calculation by a rigid 100 cm^{-1}).

In the P = 1 atm *P4/nmm*-LiOH-II phase, our calculations (see section XI for details) reproduce very well the frequency increase with pressure and the splitting between the highest IR and Raman active modes. Regarding LiOH-III, we find an excellent fit of the experimental data to the $I4_1/acd$ structure, regarding absolute frequencies, their slow decrease with pressure, the splitting between IR and Raman modes, and also the splitting between the two IR active modes that was deduced from deconvolution of the experimental IR spectrum.[18] In contrast, the other structural candidates, which feature stronger hydrogen bonds (see their discussion below), show significantly larger drops in the OH stretching modes when compared to LiOH-II, as well as much steeper pressure dependence of the peak positions and different IR/Raman splittings than seen in experiment.

We then simulated neutron diffraction patterns for LiOD. In Figure 5, we show the results for various candidate structures, together with the experimental diffraction pattern from Ref. 19, and explicit indication of the peaks discussed in that work. As can be seen, the $I4_1/acd$ structure provides an excellent fit to the data, and suggests that several other peaks in the histogram (at d = 1.63, 1.94, and 2.10 Å) do in fact also belong to LiOD, and not to the pressure cell. The $P2_1/a$ structure based on NaOD suggested in the analysis of the neutron data also fits the two largest peaks. However, after optimization of the atomic positions in that structure, the agreement is much less favorable. Other structures, including *P4/nmm*-LiOD-II and stronger hydrogen-bonded *Pbcm* do not fit the neutron data at all.

In summary, arguments based on calculated ground state enthalpies, as well as comparisons to available experimental data (on unit cell volumes, vibrational spectra, and structure factor), all strongly suggest that the high-pressure phase LiOH-III takes up the $I4_1/acd$ structure. We cannot, however, exclude that this structure is (while most likely close) not fully correct; further experimental refinement of the structure will clarify this.

Tetragonal structures of $I4_1/acd$ symmetry were suggested in other compounds of metals with first row-hydrides: for the high-pressure phase $LiBH_4$-III, based on both diffraction experiments and theory (stable between 0.9 and 27 GPa);[23,55] and as a candidate for δ-$Mg(BH_4)_2$, based on first-principles calculations (stable between 0.7 and 9.8 GPa).[56] Both share structural features with $I4_1/acd$-LiOH: in $LiBH_4$, the Li^+ cation network is simple cubic, each lithium atom is tetrahedrally coordinated in boron atoms, and each boron atom forms (very flat) square planar pyramids with lithium. In $Mg(BH_4)_2$, half as many cation sites are occupied by Mg^{2+}, which are also tetrahedrally coordinated in

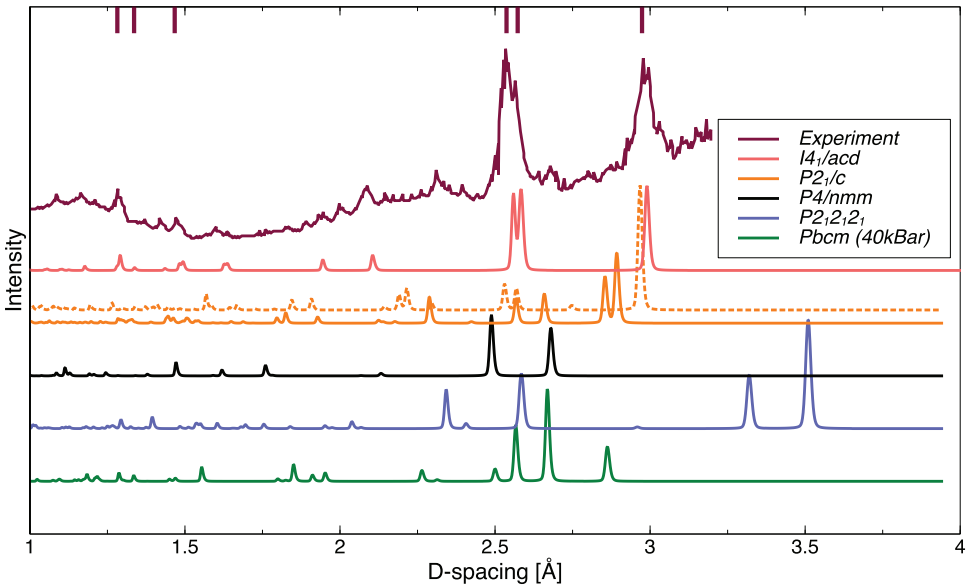

FIG. 5. Simulated neutron diffraction patterns for LiOD ground state structures, all (except *Pbcm*) at P = 2 GPa. For $P2_1$/a, the dashed (solid) line indicate diffraction patterns of the suggested NaOD-like structure before (after) optimization. Peaks discussed in the experimental room-temperature data[19] are indicated at by vertical bars at the top.

boron atoms. Naturally, neither compound features hydrogen bonds.

As the oxygen atoms in $I4_1/acd$-LiOH are very close to the plane of lithium atoms, one might wonder whether concerted and coherent proton diffusion *along* the linear hydrogen bonds (i.e., along the *a* or *b* axis), which leads to an inversion OH · · · O ↔ O · · · HO of each hydrogen bond, might be a low-barrier process. However, we find the barrier for such a process to be quite high, between 1.50 (at P = 1 atm) and 0.75 eV/formula unit (at P = 20 GPa). Another possibility would be a concerted protonic conduction *perpendicular* to the hydrogen bonds, within the *ab* plane, with protons hopping from one OH group to the next. This process has even higher barriers in the stability region of the $I4_1/acd$ structure (see the supplementary material[50] for details on this and the previous process). It is therefore likely that $I4_1/acd$-LiOH is robust against hydrogen diffusion or tunnelling processes.

Within the quasiharmonic approximation (see section XI for details), we find LiOH-III to be dynamically stable across its entire range of enthalpic stability. The P = 1 atm *P4/nmm* phase develops a dynamical instability around P = 6 GPa (see the supplementary material[50] for phonon dispersion curves), which leads to a rotation of the OH groups such that they form the hydrogen-bonded *Pbcm* phase.

VI. METASTABLE STRUCTURES AND CONNECTIONS TO OTHER SYSTEMS

We included several metastable structures in the discussion above. The first of those, of $P2_12_12_1$ symmetry, is actually the first *zig-zag* hydrogen-bonded structure that becomes more stable than the *P4/nmm* structure. Even though it never reaches absolute stability (being unstable with respect to the $I4_1/acd$ structure), it is worthwhile illustrating the structural features of such a system. In Figure 6, we show the $P2_12_12_1$ structure (see the supplementary material[50] for more views and structural analysis of the hydrogen-bonded sub-lattices), and indicate its relation to structures of the same symmetry in electronically similar systems. The first is the low-temperature phase of cesium oxydeuteride, CsOD, stable at

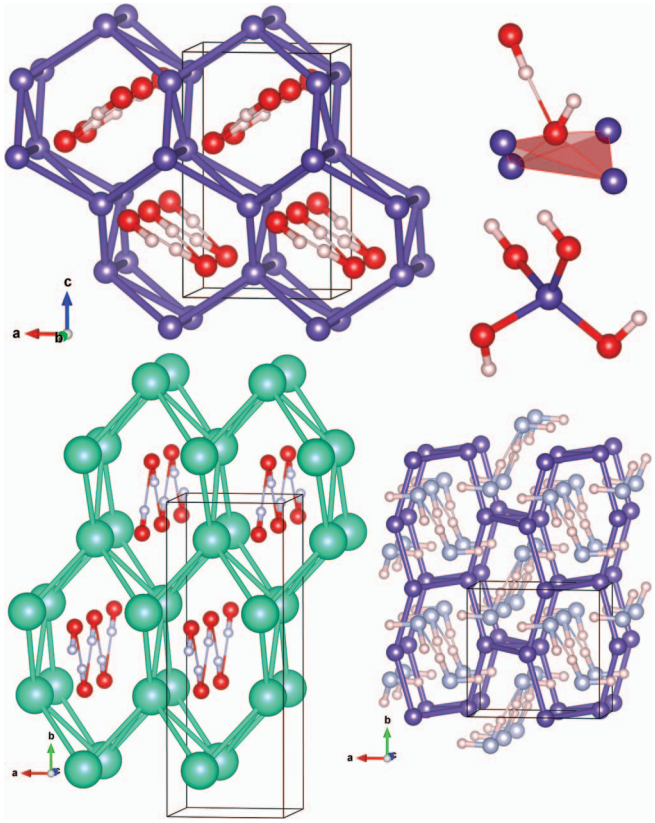

FIG. 6. Top panel: $P2_12_12_1$-LiOH at P = 10 GPa, plus coordination environments of OH and Li; bottom left: $P2_12_12_1$-CsOD at P = 1 atm; bottom right: $P2_12_12_1$-$LiNH_2$ at P = 60 GPa. Large green (small pale blue) spheres denote Cs (N) atoms.

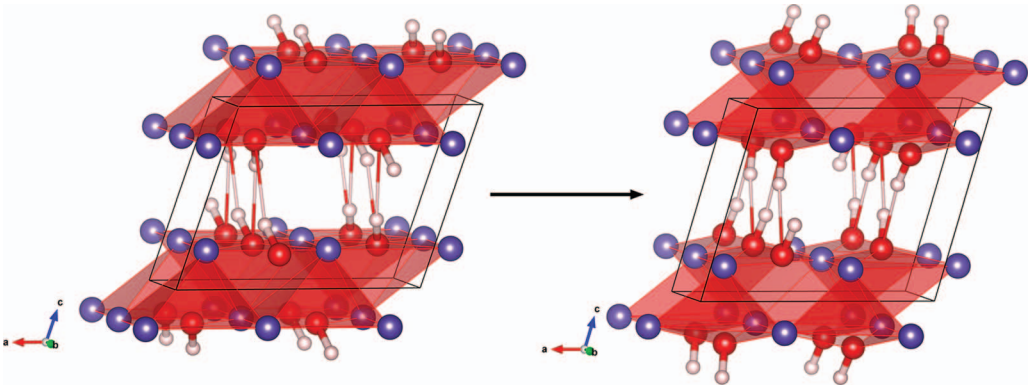

FIG. 7. The $P2_1/a$ structure as proposed at 1.8 GPa (left) and its optimized ground state at 2 GPa (right). Coordination polyhedra of oxygen are indicated in red, and hydrogen bonds by thin lines.

$T < 230$ K,[9] and the other a high-pressure phase of lithium amide, $LiNH_2$, stable in calculations between $P = 46$–280 GPa.[22] In these three structures, the cations form more or less distorted hexagonal networks, and the anions form hydrogen bonded zig-zag chains along the channels in the cation network. The detailed shape of the cation network depends on the choice of the cation as well as the external conditions (i.e., pressure). Both high-pressure phases (LiOH and $LiNH_2$) feature more close-packed herring-bone arrangements of the anion chains than CsOD, where the OD-chains are all parallel. All of these structures are inherently three-dimensional, whereas the corresponding P = 1 atm, room temperature phases of each compound are layered. In the $LiNH_2$ structure, adjacent NH_2^- units get closer to each other with increased pressure until, at around P = 500 GPa, they form infinite –(NH–H–)– chains.[22]

The $I4_1/acd$ and $P2_12_12_1$ structures are parallel in enthalpy over a significant pressure range, even though their structural characteristics seem very different, as they feature linear and zig-zag hydrogen bonds, respectively. We modelled the energy of isolated linear and bent hydrogen-bonded OH-chains (see the supplementary material[50]), and found the energy difference in the relevant O–O distance range to be roughly constant and about 0.2 eV/OH or 0.1 eV/atom; which (see Figure 2) contributes about half of the enthalpy difference between the structures. Of course, the cationic networks also differ, and hence the respective contributions to the Madelung energy of the complete structures.

Yet another phase that features zig-zag O–H · · · O–H chains, and which was proposed for LiOH-III on the basis of neutron diffraction refinement, is the $P2_1/a$ phase found at low temperatures in NaOD.[15,19] It is a layered structure with hydrogen bonds between the layers (see Figure 7). Albeit more stable than the *P4/nmm* phase at P > 8 GPa, the $P2_1/a$ phase is always metastable, because other hydrogen-bonded phases, such as the above mentioned $P2_12_12_1$ phase or the *Pbcm* phase, are more stable. We find that some of the characteristic features of this structure (as seen in NaOD) differ in LiOH: where in NaOD the hydrogen bonds are strongly non-linear, $\alpha_{O\text{–}H\cdots O} = 151^\circ$, and oxygen is five-fold coordinated in sodium, in LiOH the hydrogen bonds are quasi-linear, $\alpha_{O\text{–}H\cdots O} = 173^\circ$, and the coordination of oxygen in lithium reduces to four-fold during the optimization, see Figure 7. This rather significant reorganisation of the structure is responsible for the notably worse agreement of the optimized $P2_1/a$ phase with the neutron diffraction data in Figure 5.

Because of the ionic character of LiOH, one can conceive potential high-pressure structures based on other isoelectronic systems: from the LiF rocksalt structure[57] by substituting F with OH; from the BeO wurtzite structure[58] by substituting Be → Li and O → OH; or the *Bmmb*-HF structure[59] by HF → OH and adding lithium in cavities in the structure. None of those substitutions revealed new stable phases, but some relaxed towards metastable structures that had been found in our structure search.

VII. TRANSITION TO LiOH-IV AND BEYOND

At P = 16.5 GPa, we find a new structure of *Pbcm* symmetry becoming more stable than $I4_1/acd$, and remaining as such up to P = 1100 GPa. We thus propose a new high-pressure phase, LiOH-IV, above about 17 GPa. High-pressure phases of *Pbcm* symmetry have been found in *all* of NaOH, KOH, and RbOH (although their structures are not necessarily identical),[21] and the *Pbcm*-NaOH/-NaOD phase was described as a distorted NiAs-type structure,[20,42] with Na^+ and OH^- occupying the respective sites. The same can be said about *Pbcm*-LiOH: the OH groups form a hexagonal close-packed sublattice, with the lithium atoms interspersed and forming a simple hexagonal sublattice. Each OH group is surrounded by an octahedron of lithium atoms, and each lithium atom is coordinated to a trigonal antiprism of OH groups (see Figure 8). All OH groups lie within the hexagonal basal plane, where they form one-dimensional zig-zag chains of hydrogen bonds.

A variety of other phases are only slightly higher in enthalpy than this *Pbcm* phase across a wide pressure range, see Figure 9. These phases (also shown in Figure 8) are all structurally very similar to *Pbcm*, and differ in the relative orientation of the OH groups (and hence the hydrogen bond network) throughout the crystal. Their structures are also listed in the supplementary material.[50]

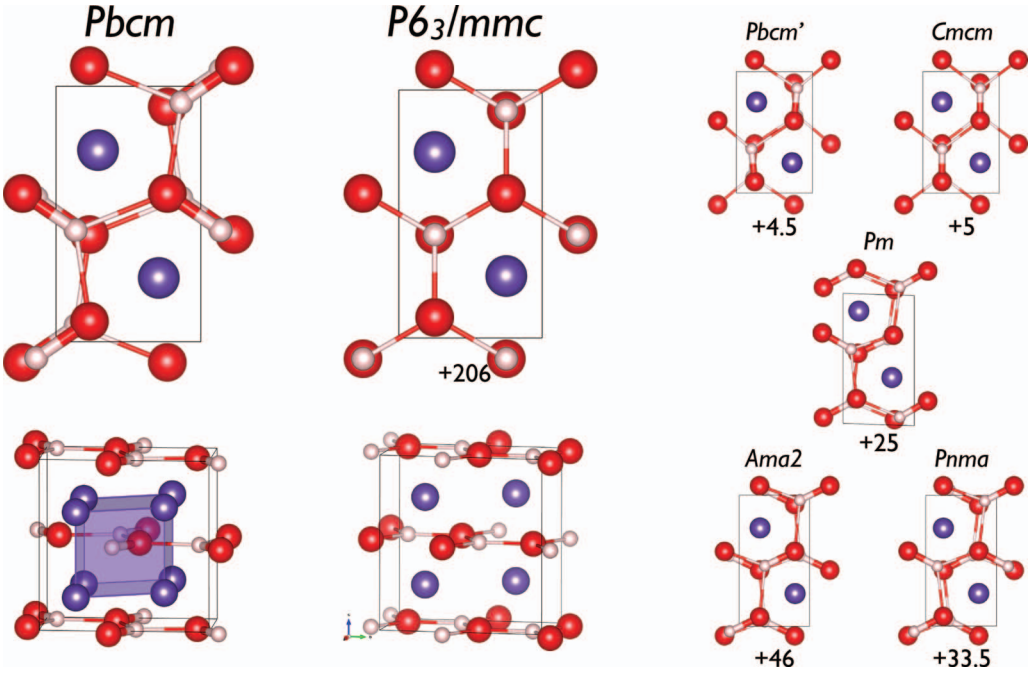

FIG. 8. From left: *Pbcm* structure of LiOH-IV, top and side view with OH coordination environment; the high-symmetry atomic $P6_3/mmc$ phase in the same views; and the five *other* distortions of $P6_3/mmc$, top views. Numbers indicate metastability per formula unit at P = 300 GPa with respect to *Pbcm*-LiOH-IV.

In fact, all of those structures can be interpreted as Peierls distortions of a high-symmetry $P6_3/mmc$ phase with graphitic sheets of OH, see Figure 8, which is then isostructural and isoelectronic to the boron-carbon sub-lattice in LiBC.[60] Such a two-dimensional atomic network of oxygen and hydrogen would then be a new structural motif for combinations of these two elements. At moderately high pressures (say, 300 GPa), this structure is very unstable, energetically (see Figure 9) and also dynamically (see the supplementary material[50]). Distortions of the OH sub-lattice to form a hydrogen-bonded network of OH groups are very favorable. There are 16 crystallographically distinct such distortions in the four-molecule unit cell of $P6_3/mmc$ shown in Figure 8, and all of the resultant structures were found in our structure search, with *Pbcm* as the global minimum. The enthalpies of all these distorted structures span the shaded area in Figure 9. Optimizing all possible distortions of the OH sub-lattice in both a six- and eight-molecule super cell of $P6_3/mmc$ at P = 300 GPa did not result in any lower enthalpy structures than the *Pbcm* structure.

Figure 9 shows that the relative instability of $P6_3/mmc$ decreases with increasing pressure. Might the ground state of LiOH then eventually feature an atomic, graphitic OH sub-lattice? Indeed, at very high pressures, around P = 1100 GPa, see Figure 9, the high-symmetry polymeric $P6_3/mmc$ phase becomes the ground state of LiOH (it is also, within the quasi-harmonic approximation, dynamically stable, see the supplementary material[50]). We might tentatively call this

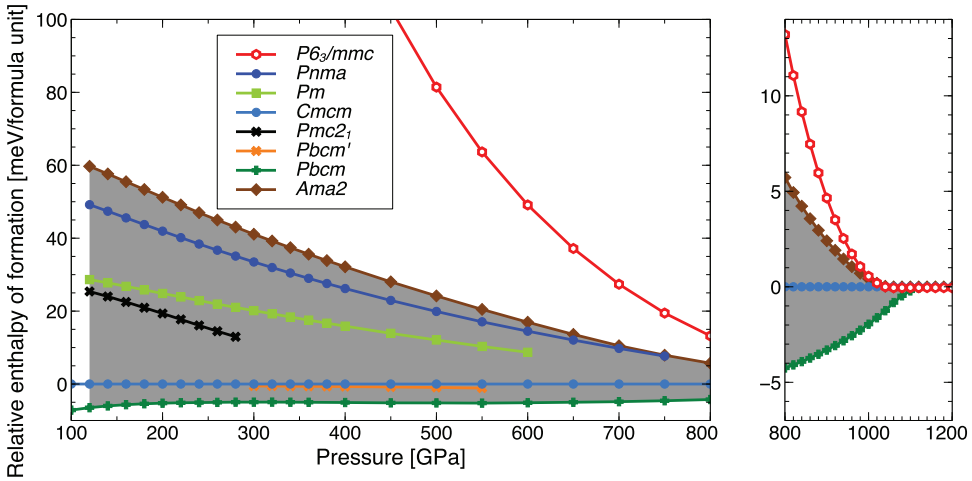

FIG. 9. Relative enthalpies of formation of high-pressure ground state phases of LiOH, with respect to the *Cmcm* phase. Note the different enthalpy scale in the two panels. See text for explanation of shaded area.

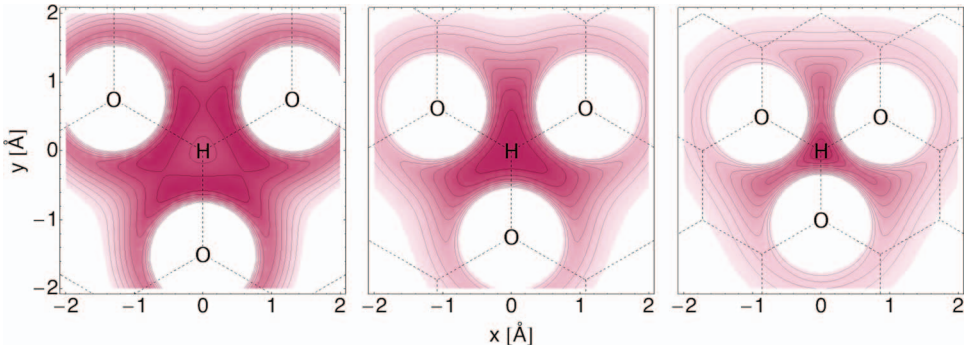

FIG. 10. Potential energy surface for a proton in a graphitic sheet of OH (ideal positions indicated). Darker colors are lower energy. From left to right: d(O-H) = 1.5, 1.25, 1.0 Å.

the LiOH-V phase. As compression increases, there simply is no room for isolated OH groups, and a symmetric position of the protons equidistant from its three nearest oxygen neighbours is preferred. This is equivalent to the molecular-atomic phase transition from ice VIII to ice X, which creates symmetric O–H–O bonds (but takes place at ∼10-fold lower pressure[61]). A simple Morse model for the O–H interaction[62] illustrates this argument, see Figure 10: at relatively large O–H distances, preferred proton positions are close to either of the oxygen atoms (to form OH groups) and off the ideal O–H connection line (to form hydrogen bonds); at reduced O–H distances, these minima merge and the energetic minimum position for the proton is in the ideal three-fold coordinated site, hence favoring the high-symmetry phase.

The transition to a polymeric ground state in LiOH is predicted to occur at significantly higher pressures than in $LiNH_2$ (which is predicted around 280 GPa,[22] formation of infinite H–(NH)– chains) or $LiBH_4$ (which is predicted around 425 GPa,[23] formation of BH_4 layers). However, dynamical effects might play a role in reducing the transition pressure: the zero-point energies (see the supplementary material[50]) are very large, about 0.77 eV/formula unit for *Pbcm*-LiOH at P = 600 GPa, which could lead to a dynamical ground state with the protons in the higher-symmetry positions. Nevertheless, it is likely very hard to verify the polymeric O-H-network in LiOH experimentally.

VIII. ENTHALPIC STABILITY

While we know that LiOH is stable at atmospheric pressure, its high-pressure phases also have to compete with other "escape routes" in the Li-O-H system. Enthalpic stability of a certain phase in a ternary phase diagram is an important indicator for its potential synthesis,[63,64] albeit neither a necessary nor a sufficient condition.

In Figure 11, we show Li–O–H phase diagrams at two pressures, P = 1 atm and P = 80 GPa. These are constructed purely from calculations, using the respective static ground state structures of the elements, the known binary and various ternary phases. A point inside the phase diagram corresponds to a certain ternary stoichiometry, while points along the edges correspond to binary phases. All vertices shown, including the corners, denote enthalpically stable phases. All unstable stoichiometries (binary or ternary) could lower their enthalpy by decomposition into the nearest stable phases in the phase diagram. Additionally, we included dashed lines and color shadings to indicate enthalpy contours with respect to the elements—so while LiH and H_2O are definitely stable, they do not have the lowest enthalpy of formation per atom in the ternary system; the ionic solid Li_2O is the thermodynamic sink here.

At P = 1 atm, we correctly identify anhydrous LiOH and its monohydrate LiOH+H_2O as stable static phases, and

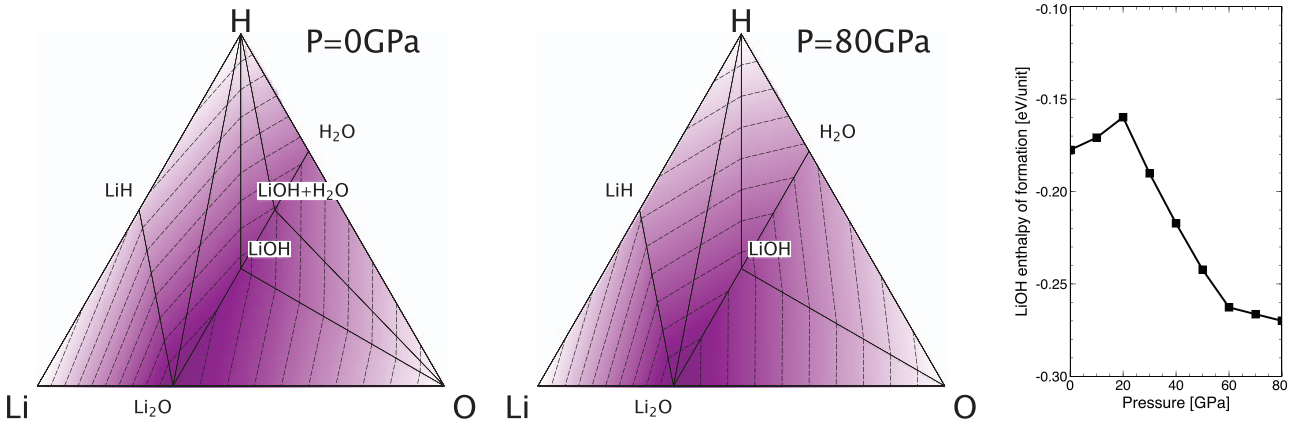

FIG. 11. From left: Ternary Li-O-H phase diagrams at P = 1 atm and P = 80 GPa (relative enthalpy of formation indicated by purple hue), and the enthalpy of formation of LiOH with respect to all competing phases.

metastable phases such as H_2O_2 are (correctly) not points of stability. At moderate pressures, between 10 and 20 GPa, LiOH+H_2O becomes metastable, while anhydrous LiOH remains a stable phase at least up to P = 80 GPa. In fact, the negative enthalpy of formation of LiOH (with respect to all positive decomposition reactions) increases in magnitude with pressure, see the right side of Figure 11. We thus expect that LiOH, once loaded into a pressure cell, could be studied up to very high pressures, including the phase transitions to LiOH-III and LiOH-IV. We note that Figure 11 uses computational results on high-pressure phases of Li_2O, LiOH+H_2O, and Li_2O+LiOH that we will discuss in a separate paper.

IX. ELECTRONIC STRUCTURE

Pure LiOH is an ionic solid, and therefore, as one might expect, a wide-gap insulator. At P = 1 atm, the DFT band gap (likely an underestimation) is 4.01 eV, and the valence bands (see Figure 12) are narrow, as the electronic states are very localized.

As expected, valence band states are dominated by OH, with lithium's 2*s* state seen in the conduction band. A topological analysis of the charge density[65] leads to a charge distribution in LiOH of $Li^{+0.84}(OH)^{-0.84}$. Interestingly, the band gap increases with pressure, and across all relevant phases (see Figure 13). In general, the more stable phases tend to feature wider band gaps.[66] However, the "ionicity" of LiOH (according to the Bader charge analysis) decreases slightly within each phase as pressure is increased. Also, the valence bands widen, in particular when hydrogen bonds are formed, see the supplementary material.[50]

Regarding a possible lowering of the metallization pressure in LiOH compared to H_2O, because of the introduction of the more electropositive lithium ions, this material seems to behave just the opposite: at P = 1200 GPa, in the polymeric *P6₃/mmc* phase, LiOH has a DFT band gap of 10.93 eV—much larger than the 5.5 eV band gap in the $Pmc2_1$ phase of ice at the same pressure.[25] The reason is the ionic component in the solid-state bonding in LiOH, which is even more pronounced than in H_2O, and means electronic charge is very localized, even up to the highest pressures studied here.

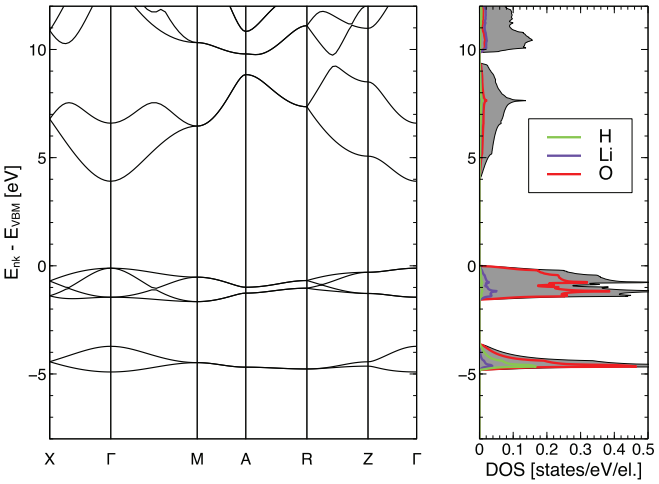

FIG. 12. Electronic band structure and DOS of *P4/nmm*-LiOH at P = 1 atm. Partial DOS of the atoms are indicated: red (green, purple) indicate oxygen (hydrogen, lithium).

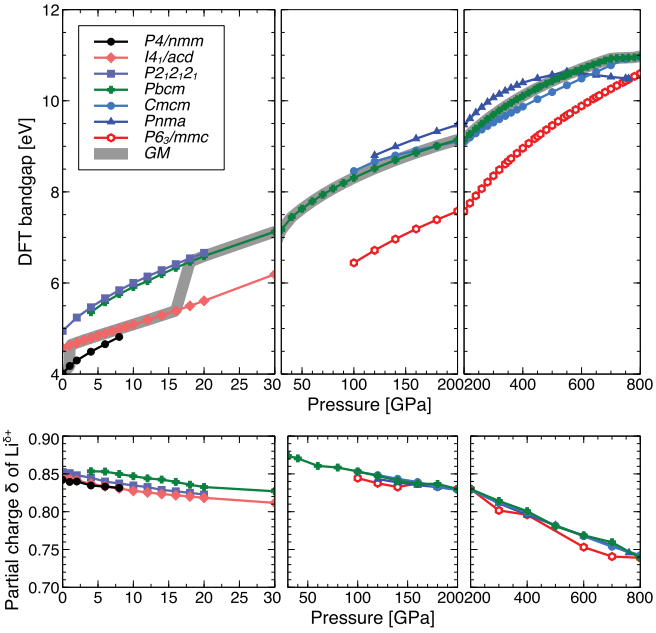

FIG. 13. Evolution of band gap and ionicity (as measured by Bader partial charge on Li) with increased pressure, across the relevant phases. "GM" indicates the global minimum.

X. SUMMARY

We have presented results of a computational study of the high-pressure phases of LiOH. We propose a re-assignment of the LiOH-III phase, which we find to be the ground state between P = 1 · · · 17 GPa. LiOH-III takes up a new tetragonal structure type amongst the alkali hydroxides with linear hydrogen-bonded OH · · · OH · · · OH chains, which order anti-ferroelectrically. Suggestive on energetic grounds, this structure also provides a better fit than those proposed previously to explain neutron diffraction and vibrational data. Another high-pressure phase, LiOH-IV, with *Pbcm* symmetry and a more common zig-zag hydrogen bond network of OH units, becomes stable for P > 17 GPa. This suggests that *all* alkali hydroxides have a high-pressure phase of *Pbcm* symmetry, even though it is not clear yet whether they are all identical. At very high pressures (P ∼ 1.1 TPa), LiOH-IV approaches a high-symmetry hexagonal structure with an unusual graphitic net of oxygen and hydrogen. The ionic character of the compound means a strong resistance to metallization, with electronic band gaps increasing up to the highest pressures studied here.

XI. COMPUTATIONAL METHODOLOGY

Density functional calculations used the PBE exchange-correlation functional[67] and regular k-point meshes of linear density 20/Å^{-1}. Low-pressure calculations (P ≤ 30 GPa) were performed with Li($2s^1$)O($2s^2 2p^4$)H($1s^1$) valence

PAW datasets with cutoff radii Li(2.05)O(1.52)H(1.10) a_B and plane-wave cut-off $E_c = 600$ eV. High-pressure calculations were performed with valence PAW datasets $Li(1s^2 2s^1)O(2s^2 2p^4)H(1s^1)$ with cutoff radii Li(1.7)O(1.1)H(0.8) a_B and plane-wave cutoff $E_c = 1000$ eV. The all-electron PAW wave functions satisfy Kato's cusp theorem at the nuclei,[68] in contrast to, e.g., ultrasoft pseudopotentials. DOS calculations used k-point meshes with densities of at least $80/Å^{-1}$. IR/Raman frequencies were calculated using the finite difference method, and symmetries of modes were determined using the QuantumESPRESSO code.[69] Phonon dispersion curves and DOS's were calculated using the PHON package, based on the finite displacement method, in supercells of at least 192 atoms.[70] Neutron diffraction pattern were simulated using the GSAS/EXPGUI software.[71,72]

ACKNOWLEDGMENTS

Funding from NSF Grant Nos. CHE-0910623 and DMR-0907425, the DoE Energy Frontier Research Center EFree (Award DESC0001057), and computational resources from XSEDE (provided by the National Center for Supercomputing Applications through NSF Grant No. TG-DMR060055N) and HECToR/ARCHER (provided by the UK National Supercomputing Service through the UKCP consortium and funded by EPSRC Grant No. EP/K013564/1) are gratefully acknowledged. A.H. wants to thank John Loveday and Dmitri Sokolov for help with simulations of neutron diffraction patterns.

[1] B. W. Hotten and D. H. Birdsall, J. Colloid Sci. **7**, 284 (1952).
[2] D. A. Boryta and A. J. Maas, Ind. Eng. Chem. Process Des. Dev. **10**, 489 (1971).
[3] G. G. Vurek, D. G. Warnock, and R. Corsey, Anal. Chem. **47**, 765 (1975).
[4] N. W. Alcock, Acta Cryst. B **27**, 1682 (1971).
[5] K. Hermansson and J. O. Thomas, Acta Crystallogr., Sect. B: Struct. Crystallogr. Cryst. Chem. **38**, 2555 (1982).
[6] S. Göttlicher and B. Kieselbach, Acta Cryst. A **32**, 185 (1976).
[7] H.-J. Bleif and H. Dachs, Acta Crystallogr., Sect. A **38**, 470 (1982).
[8] B. Mach, H. Jacobs, and W. Schäfer, Z. Anorg. Allg. Chem. **553**, 187 (1987).
[9] H. Jacobs, B. Mach, B. Harbrecht, H.-D. Lutz, and J. Henning, Z. Anorg. Allg. Chem. **544**, 55 (1987).
[10] H. Jacobs, B. Mach, H.-D. Lutz, and J. Henning, Z. Anorg. Allg. Chem. **544**, 28 (1987).
[11] J. B. Yang, X. D. Zhou, Q. Cai, W. J. James, and W. B. Yelon, Appl. Phys. Lett. **88**, 041914 (2006).
[12] W. I. F. David, M. O. Jones, D. H. Gregory, C. M. Jewell, S. R. Johnson, A. Walton, and P. P. Edwards, J. Am. Chem. Soc. **129**, 1594 (2007).
[13] J. A. Ibers, J. Kumamoto, and R. G. Snyder, J. Chem. Phys. **33**, 1164 (1960).
[14] M. A. White and S. A. Moore, J. Chem. Phys. **85**, 4629 (1986).
[15] T. J. Bastow, M. M. Elcombe, and C. J. Howard, Solid State Commun. **57**, 339 (1986).
[16] T. J. Bastow, M. M. Elcombe, and C. J. Howard, Solid State Commun. **59**, 257 (1986).
[17] T. J. Bastow, M. M. Elcombe, and C. J. Howard, Solid State Commun. **62**, 149 (1987).
[18] D. M. Adams and J. Haines, J. Phys. Chem. **95**, 7064 (1991).
[19] D. M. Adams, A. G. Christy, and J. Haines, J. Phys. Chem. **96**, 8173 (1992).
[20] H. P. Beck and G. Lederer, J. Chem. Phys. **98**, 7289 (1993).
[21] J. W. Otto and W. B. Holzapfel, J. Phys.: Condens. Matter **7**, 5461 (1995).
[22] D. L. V. K. Prasad, N. W. Ashcroft, and R. Hoffmann, J. Phys. Chem. A **116**, 10027 (2012).
[23] Y. Yao and D. D. Klug, Phys. Rev. B **86**, 064107 (2012).
[24] A. Hermann and P. Schwerdtfeger, Phys. Rev. Lett. **106**, 187403 (2011).
[25] A. Hermann, N. W. Ashcroft, and R. Hoffmann, Proc. Natl. Acad. Sci. U.S.A. **109**, 745 (2012).
[26] A. Hermann, N. W. Ashcroft, and R. Hoffmann, Phys. Rev. B **88**, 214113 (2013).
[27] E. Zurek, R. Hoffmann, N. W. Ashcroft, A. R. Oganov, and A. O. Lyakhov, Proc. Natl. Acad. Sci. U.S.A. **106**, 17640 (2009).
[28] P. Baettig and E. Zurek, Phys. Rev. Lett. **106**, 237002 (2011).
[29] J. Hooper and E. Zurek, J. Phys. Chem. C **116**, 13322 (2012).
[30] D. Lonie, J. Hooper, B. Altintas, and E. Zurek, Phys. Rev. B **87**, 054107 (2013).
[31] H. Wang, J. S. Tse, K. Tanaka, T. Iitaka, and Y. Ma, Proc. Natl. Acad. Sci. U.S.A. **109**, 6463 (2012).
[32] H. Dachs, Z. Krist. **112**, 60 (1959).
[33] S. L. Mair, Acta Crystallogr., Sect. A **34**, 542 (1978).
[34] S. Elschner and T. J. Bastow, Solid State Commun. **60**, 75 (1986).
[35] P. W. R. Bessonette and M. A. White, J. Chem. Phys. **110**, 3919 (1999).
[36] J. M. Kiat, G. Boemare, B. Rieu, and D. Aymes, Solid State Commun. **108**, 241 (1998).
[37] V. A. Khitrov, N. N. Khitrova, and V. F. Khmelkov, Zhur. Obs. Khim. USSR **23**, 1630 (1953).
[38] P. A. Kollman, J. F. Liebman, and L. C. Allen, J. Am. Chem. Soc. **92**, 1142 (1970).
[39] S. F. Smith, J. Chandrasekhar, and W. L. Jorgensen, J. Phys. Chem. **86**, 3308 (1982).
[40] A. B. Sannigrahi, T. Kar, B. G. Niyogi, P. Hobza, and P. von Rague Schleyer, Chem. Rev. **90**, 1061 (1990).
[41] M. P. Krobok and W. B. Holzapfel, J. Phys.: Condens. Matter **6**, 9789 (1994).
[42] J. S. Loveday, W. G. Marshall, R. J. Nelmes, S. Klotz, G. Hamel, and J. M. Besson, J. Phys.: Condens. Matter **8**, L597 (1996).
[43] R. Martoňák, A. Laio, and M. Parrinello, Phys. Rev. Lett. **90**, 075503 (2003).
[44] R. Martonák, D. Donadio, A. R. Oganov, and M. Parrinello, Nat. Mater. **5**, 623 (2006).
[45] M. Pagliai, M. Iannuzzi, G. Cardini, M. Parrinello, and V. Schettino, ChemPhysChem **7**, 141 (2006).
[46] D. C. Lonie and E. Zurek, Comput. Phys. Commun. **182**, 372 (2011).
[47] D. C. Lonie and E. Zurek, Comput. Phys. Commun. **183**, 690 (2012).
[48] G. Kresse and J. Furthmüller, Phys. Rev. B **54**, 11169 (1996).
[49] G. Kresse and D. Joubert, Phys. Rev. B **59**, 1758 (1999).
[50] See supplementary material at http://dx.doi.org/10.1063/1.4886335 for crystal structures, hydrogen bond analysis, electronic band structures, phonon dispersions, and pseudopotential tests.
[51] H. Tanigawa and S. Tanaka, J. Nucl. Sci. Technol. **38**, 1004 (2001).
[52] M. Mérawa, P. Labeguerie, P. Ugliengo, K. Doll, and R. Dovesi, Chem. Phys. Lett. **387**, 453 (2004).
[53] G. Gajewski, P. D. Mitev, and K. Hermansson, J. Chem. Phys. **129**, 064502 (2008).
[54] K. Azuma, T. Oda, and S. Tanaka, Comput. Theor. Chem. **963**, 215 (2011).
[55] S. Nakano, H. Fujihisa, H. Yamawaki, Y. Gotoh, and T. Kikegawa, Rev. High Press. Sci. Technol. **21**, 213 (2011).
[56] X. Zhou, A. R. Oganov, G.-R. Qian, and Q. Zhu, Phys. Rev. Lett. **109**, 245503 (2012).
[57] J. Thewlis, Acta Crystallogr. **8**, 36 (1955).
[58] D. K. Smith, H. W. Newkirk, and J. S. Kahn, J. Electrochem. Soc. **111**, 78 (1964).
[59] M. Atoji and W. N. Lipscomb, Acta Crystallogr. **7**, 173 (1954).
[60] M. Wörle, R. Nesper, G. Mair, M. Schwarz, and H. G. von Schnering, Z. Anorg. Allg. Chem. **621**, 1153 (1995).
[61] R. Caracas, Phys. Rev. Lett. **101**, 085502 (2008).
[62] W. B. Holzapfel, J. Chem. Phys. **56**, 712 (1972).
[63] A. Hermann, B. L. Ivanov, N. W. Ashcroft, and R. Hoffmann, Phys. Rev. B **86**, 014104 (2012).
[64] D. J. Frederman, P. H. Tobash, M. A. Torrez, J. D. Thompson, E. D. Bauer, F. Ronning, W. W. Tipton, S. P. Rudin, and R. G. Hennig, Phys. Rev. B **83**, 224102 (2011).
[65] R. F. W. Bader, *Atoms in Molecules: A Quantum Theory* (Oxford University Press, 1994).

[66]R. G. Pearson, Acc. Chem. Res. **26**, 250 (1993).
[67]J. P. Perdew, K. Burke, and M. Ernzerhof, Phys. Rev. Lett. **77**, 3865 (1996).
[68]T. Kato, Commun. Pure Appl. Math. **10**, 151 (1957).
[69]P. Giannozzi, S. Baroni, N. Bonini, M. Calandra, R. Car, C. Cavazzoni, D. Ceresoli, G. L. Chiarotti, M. Cococcioni, I. Dabo, A. Dal Corso, S. de Gironcoli, S. Fabris, G. Fratesi, R. Gebauer, U. Gerstmann, C. Gougoussis, A. Kokalj, M. Lazzeri, L. Martin-Samos, N. Marzari, F. Mauri, R. Mazzarello, S. Paolini, A. Pasquarello, L. Paulatto, C. Sbraccia, S. Scandolo, G. Sclauzero, A. P. Seitsonen, A. Smogunov, P. Umari, and R. M. Wentzcovitch, J. Phys.: Condens. Matter **21**, 395502 (2009).
[70]D. Alfè, Comput. Phys. Commun. **180**, 2622 (2009).
[71]A. C. Larson and R. B. Von Dreele, General Structure Analysis System (GSAS), Los Alamos National Laboratory Report LAUR 86-748 (1994).
[72]B. H. Toby, J. Appl. Crystallogr. **34**, 210 (2001).